NANO LETTERS

Probing Rotational and Translational Diffusion of Nanodoublers in Living Cells on Microsecond Time Scales

Carlos Macias-Romero,[†] Marie E. P. Didier,[†] Vitalijs Zubkovs,[†] Lucas Delannoy,[†,‡] Fabrizia Dutto,[‡] Aleksandra Radenovic,*[,‡] and Sylvie Roke*[,†]

[†]Laboratory for Fundamental BioPhotonics and [‡]Laboratory of Nanoscale Biology, Institute of Bioengineering, École Polytechnique Fédérale de Lausanne (EPFL), 1015, Lausanne, Switzerland

Ⓢ Supporting Information

ABSTRACT: Nonlinear microscopes have seen an increase in popularity in the life sciences due to their molecular and structural specificity, high resolution, large penetration depth, and volumetric imaging capability. Nonetheless, the inherently weak optical signals demand long exposure times for live cell imaging. Here, by modifying the optical layout and illumination parameters, we can follow the rotation and translation of noncentrosymmetric crystalline particles, or nanodoublers, with 50 μs acquisition times in living cells. The rotational diffusion can be derived from variations in the second harmonic intensity that originates from the rotation of the nanodoubler crystal axis. We envisage that by capitalizing on the biocompatibility, functionalizability, stability, and nondestructive optical response of the nanodoublers, novel insights on cellular dynamics are within reach.

KEYWORDS: *Nonlinear microscopy, second harmonic generation, nanodoublers, particle tracking, translational and rotational diffusion*
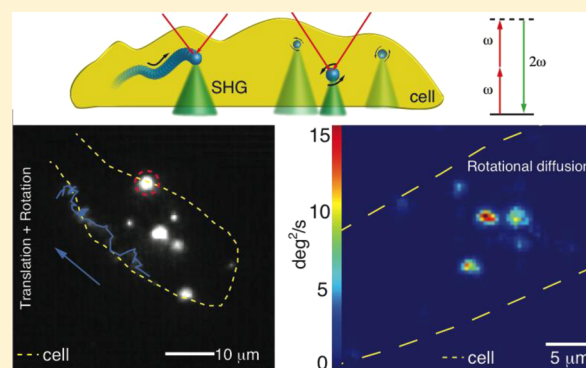
Cellular functions rely on a complex network of pathways and dynamic processes. To study dynamical processes such as membrane transport, translocation and formation, axonal transport, and drug delivery, it is often necessary to insert foreign bodies as probes that can be chemically and selectively linked to one of the actors to follow the process by optical imaging.[1−5] Ideal tracking probes should not saturate, blink, nor photobleach,[6] and they should not be destructive or toxic to the embedded environment. The probe should be sufficiently small to not disrupt the process under study (100 nm or smaller) and have a narrow spectral bandwidth and a bright emission spectrum.[7−9] The probe should also be biocompatible and functionalizable. In order to obtain a complete map of the dynamics under study, both the translation and the rotation of the probe should be followed on ideally microsecond time scales (which is the typical time scale of rotational diffusion). To date, those aspects have not been met in wide field live cell imaging. Here, we follow the rotation and translation of nanodoublers in vitro with 50 μs acquisition time per image. The rotational diffusion is derived from variations in the second harmonic intensity that originates from the rotations of the principal axis of the nanodoubler.

In recent years, many advances have been made both in terms of imaging systems and probe development. An imaging system dedicated to translational and rotational tracking should ideally have image acquisition times that are faster than the translational and rotational motion of a nanoparticle ($\ll$1 ms)

and allow for a simultaneous observation of a large field of view (>2000 μm^2). Current state-of-the-art tracking imaging systems include one-photon fluorescent microscopes in confocal,[10] total internal reflection fluorescence (TIRF)[11,12] and epi[13,14] configuration, dark-field linear scattering,[15,16] photothermal imaging,[17] difference interference contrast microscopy,[2,3,18−20] linear[21,22] and nonlinear[23] correlation spectroscopy, two-photon, single-[24] and multi-confocal microscopy,[25] planar illumination,[26] linear TIR scattering,[27] defocused wide field,[28] nonlinear holographic imaging,[29] and scanning second harmonic microscopy.[30−35] Linear in vitro imaging of gold nanorods with CMOS technology[2] can reach image acquisition times of 2 ms. Second harmonic imaging of nanodoublers has been performed with a 50 ms acquisition time per image for fixed nanodoublers and with a 1 s acquisition time per image for in vivo imaging.[35] In general, the image acquisition time for second harmonic imaging is commonly slower because of the weak nonlinear optical response and the subsequent need to scan a tight focus in order to overcome low signal-to-noise ratios.

For the probes, fluorescent molecules,[1] metallic nanoparticles,[1,2,25] quantum dots,[5,36] nanodiamonds,[10] and nanodoublers[9,23,24,30,32,33,35,37−44] are available. While it is possible
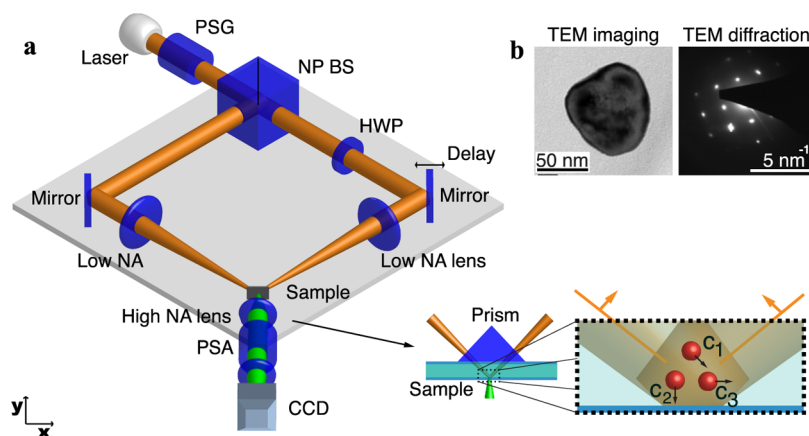
Figure 1. Principles of the method. (a): Optical scheme of the second harmonic microscope, showing a sketch of the sample chamber and beam geometry in the inset. NA stands for numerical aperture, PSA for polarization state generator, HWP for half wave plate, NP BS for nonpolarizing beam splitter. The magnified inset shows the sample chamber with an illustration of the principle behind the measurement of the nanodoubler rotation. The black arrows indicate the orientation of the principal axis of the crystal. The brightness of the nanodoublers in the image depends on the relative angle between their crystal axis and the electric field direction of the laser beam. The orange arrows depict the polarization state of the beams. A detailed description of the angles and formula can be found in the Supporting Information. (b) Transmission electron microscopy images and diffraction pattern of a single $KNbO_3$ nanoparticle as a measure to determine its degree of crystallinity. More data on the particle characterization can be found in the Supporting Information.

to track the translation of all these probes, the rotation can only be observed if some kind of geometrical or optical anisotropy is present. Nonspherical fluorescent molecules,[4,11,12,14] quantum rods,[13] and metallic nanorods[2,3,15−17,19−22,25−28] are typically the preferred candidates for this purpose, using the anisotropy resulting from the aspect ratio of the object. Optical imaging combined with the detection of magnetic spin echo decay in nanodiamonds[10] is another approach toward tracking of translation and rotation. Nanodoublers are particles with a noncentrosymmetric crystal lattice structure. When a nanodoubler interacts with an optical beam with frequency ω, it emits light with a frequency 2ω with a spectral width that is determined by the spectral width of the incident optical beam. This second harmonic generation process is elastic; saturation and photobleaching are absent, allowing for measurements during indefinite periods of time. Nanodoublers can also be easily functionalized with, for example, proteins[7,41,45,46] for targeting[47] specific biological questions.[7−9,37,45,47,48]

Here, we demonstrate the possibility to track the translation and rotation of nanodoublers in living cells with image acquisition times as low as 50 μs per image. After introducing the imaging system and particle characterization, we show the translational diffusion of functionalized 100 nm $KNbO_3$ nanodoublers in water and inside living cells, paying attention first to the translational and then to the rotational motion of the nanodoublers.

Imaging System and Particle Characterization. Figure 1a shows an illustration of the wide field illumination scheme used here (further details about the used angles can be found in Supporting Information Figure S1). The two weakly focused beams create an elliptical illumination spot with diameters of 100 and 140 μm, and an illumination depth of 70 μm. The area of the field of view is 5674.5 μm^2, which is determined by the 190 fs pulse duration of the beams. The light source consists of a 200 kHz Yb:KGW amplified laser delivering 1028 nm pulses with a duration of 190 fs. The pulse energies used in the experiment (and measured at the focus) are in the range of 0.3−0.8 μJ, which corresponds to a fluence (~2.7−7.2 mJ/cm^2) well below the damage threshold of living (CHO) cells. As an

example, full cell viability in CHO cells was retained after irradiation[49] with 100 kHz repetition rate 1035 nm laser pulses in a confocal illumination geometry up to a fluence of[2] 119 mJ/cm. This value is, however, dependent on the quality of the optical beam, cell type and tissue. The objective lens (50×, 0.65 NA) has a field of view that is larger than the illumination area, and it is placed along the phase-matched direction of the two incoming beams. Detection is done with a gated-intensified charge-coupled device camera (CCD). The double beam geometry allows one to probe multiple polarization combinations and ensures that the objective lens is not damaged. The optical resolution can be similar to that of the confocal homologous.[50] A wide field geometry with two weakly focused beams has been proposed recently by Peterson et al.[51] who used a 1 kHz 800 nm fs amplifier as light source and a CCD camera as detector. They imaged sugar and CdSe quantum dots with image acquisition times between 3 and 10 min.[51] We use a different light source and gated detection and have added a prism for efficient coupling and to reduce polarization aberrations.

The nanodoublers used in our study are $KNbO_3$ crystalline particles that are coated with polyethylene glycol (PEG).[9] The particle size distribution was measured by dynamic light scattering (DLS) in water and cell serum, which showed an average particle diameter of ~107 nm with a polydispersity index of 12% (see Supporting Information, Figure S2). The particles were further characterized by transmission electron microscopy (TEM) in imaging and diffraction mode (see Figure 1b and further images in the Supporting Information, Figure S3). The TEM diffraction images show that the particles are highly crystalline, while the TEM images show that the particles have an irregular shape. Because the DLS size distribution in solution is narrow and the TEM images display different irregularities per particle (see Supporting Information), we approximate the particle shape as spherical, which we will need to calculate the rotational diffusion.

Translational Diffusion of Nanodoublers in Water. We first explore the diffusion of 100 nm $KNbO_3$ nanodoublers[9] in pure water at room temperature (293 K). A nanodoubler
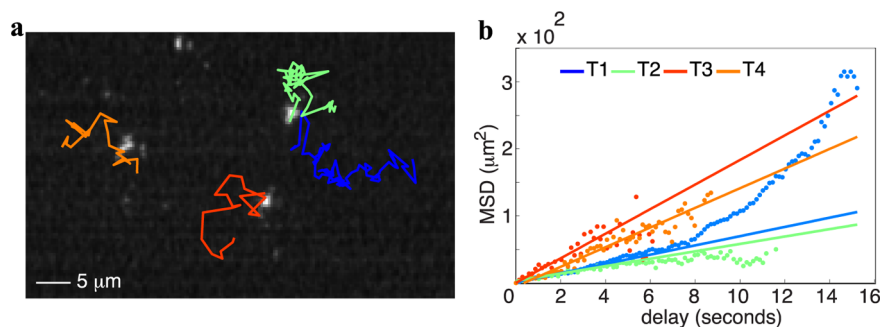
Figure 2. Translational diffusion of 100 nm $KNbO_3$ particles in water. (a) A frame taken from a movie of nanodoublers diffusing in water (see Supporting Information Movie 1). The solid lines in (a) depict the tracks of four particles. The MSD of these tracks is shown as colored data points in (b). The solid lines in (b) represent the corresponding linear fit to each MSD using the first 15% of the maximum delay of the data. The image acquisition time is 250 μs and the particles are confined to a chamber 5 μm in depth.

dispersion of 3 μg/mL is inserted in the flow chamber (5 μm in depth) and the trajectories of the particles are recorded with 250 μs acquisition time per frame. Figure 2a shows a frame taken from a typical movie with the tracks superimposed. Figure 2b shows the mean square displacement (MSD) calculations and the corresponding fits to a Brownian diffusion model.[52] One can see from the MSD (Figure 2b) that apart from the blue track (T1), which follows a driven motion, the rest of the particles follow approximately a Brownian motion.[52] The extracted diffusion coefficient of 20 tracks was 4.88 ± 0.59 μm^2/s. Given the small irregularities in the particles shape, this is in excellent agreement with the expected translational diffusion of 4.80 μm^2/s for 100 nm spherical particles in water. For the four tracks displayed in Figure 2, the measured mean diffusion coefficient is 4.89 ± 1.49 μm^2/s. From the images it can be seen that the intensity distribution is uniform across each particle. The DLS data (see Supporting Information Figure S2) shows that the solution contains single particles and no clusters. As the height of the flow chamber (5 μm) is smaller than the illumination depth (70 μm) all particles are in focus. The observed intensity variations can be related to particle rotation, as we will show below.

Next, we explore the options for in vitro imaging. We first focus on the translational motion and the response of the cell to the foreign body (with an acquisition time of 25 ms per image) and then on the rotational dynamics of particles (with an acquisition time of 50 μs per image).

Time Resolved in Vitro Imaging. Figure 3 demonstrates the possibilities of time resolved imaging of processes within living cells. Human epitheloid cervix carcinoma (HeLa) cells were electroporated with 100 nm diameter $KNbO_3$ particles. Figure 3a shows a phase contrast image, and Figure 3b shows a time-integrated stack of second harmonic images of the cells containing the particles. The corresponding movie can be found in the Supporting Information (Movie 2). Three dimensional confocal two photon fluorescence/second harmonic imaging of Nile red stained HeLa cells containing the nanoparticles showed that the particles are inside the cell. The images and a more complete description of the experiment are included in the Supporting Information. The arrow in Figure 3b points toward the motion of the selected nanodoubler. It can be seen that the cell has immobilized the particle encircled in red and that another particle appears to interact with the cell membrane, which is possibly being ejected by the cell (blue path). The translational mean square displacement is shown in Figure 3c. Compared to Brownian motion in water (indicated
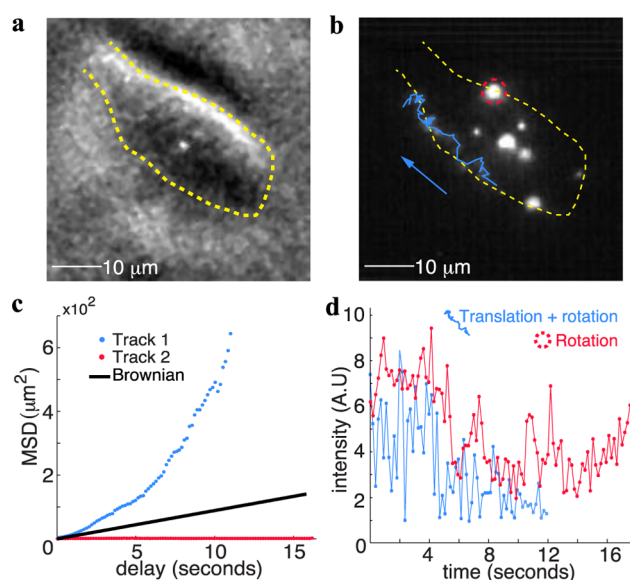

Figure 3. Time resolved nanoparticle tracking. Phase contrast image (a) and second harmonic image stack (b) of human epithelial cervix carcinogenic cells transfected with 100 nm diameter $KNbO_3$ nanodoublers. The image in (b) is a time-averaged stack depicting in blue the track of a particle diffusing and rotating and a particle rotating encircled in red. The movie provided in the Supporting Information (Movie 2) displays the moving particle interacting with the membrane before continuing its path (blue track), and the rotation of the particle encircled in red. The mean square displacement (MSD) of each particle is shown in (c). It can be seen that the particle motion deviates significantly from Brownian motion for both cases. The intensity of the two nanodoublers is shown in (d) as a function of time. The intensity fluctuations are caused by rotational motion.

by the black curve), both particle tracks display a difference from normal diffusion. While the particle in red is not moving, the particle in blue follows a driven diffusion that is significantly faster (12.18 μm^2/s) compared to Brownian diffusion in water (4.80 μm^2/s). This significant difference might suggest that the particle is being ejected by the cell. The intensity of both particles is displayed as a function of time in Figure 3d, fluctuating on a scale of 1−10. As the standard error to the mean in our setup is 1−2%[53] (which leaves the system shot-noise limited), we can exclude instrumentation errors as the source of the fluctuations. The significant variation in intensity is caused by particle rotation: The intensity of monocrystalline nanodoublers strongly depends on the orientation of the

particle crystalline axis relative to the electric field of the illuminating beams (as sketched in the inset of Figure 1 and shown in more detail in Supporting Information Figure S6). If the main crystalline axis of the particle is perpendicular to the oscillation direction of the input electric fields, no SH light is emitted (see Supporting Information Figure S6c for the theoretical calculations of the intensities). Vice versa, maximum SH emission is obtained when both are parallel. The same principle holds for our beam geometry. The Supporting Information contains the formulas used to relate the intensity to the rotation of the nanodoublers. The intensity variations observed here correspond to those observed for immobilized particles illuminated with rotating polarization. This data is included in the Supporting Information (Figure S5). The intensities of Figure 3 are similar in value as those in Figure 2, and the intensity distribution across the particles is also uniform, indicating that we are measuring single particles. Because the scattered second harmonic intensity from a particle or cluster is strongly size dependent,[54] clusters will have significantly larger intensities and are likely not present in the image. It is further interesting to note that the analysis of the rotational motion of nanodoublers using the temporal intensity profiles has been predicted previously.[30−32,38] In order to map the rotational diffusion more accurately we image nanodoublers in vitro with shorter acquisition times.

Figure 4 shows the rotational diffusion of the nanodoublers in vitro with integration times of 50 μs, together with a spatial map of the rotational diffusion coefficient. The corresponding movie can be found in the Supporting Information (Movie 3). Here, HeLa cells were again electroporated with the 100 nm KNbO$_3$ particles and a movie was recorded with 50 μs
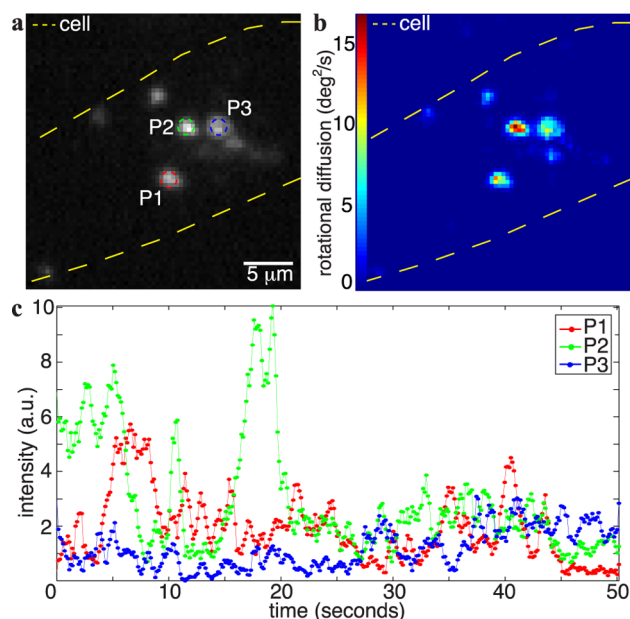

Figure 4. Spatial mapping of the rotational diffusion of 100 nm KNbO$_3$ nanodoublers inside a living cell. (a) Second harmonic signal of the intensity integrated over all the frames of a movie taken (see Movie 3 in the Supporting Information) with an acquisition time per frame of 50 μs. (b) Spatial map of the rotational diffusion obtained from the relation between the variations in intensity and the rotation of the nanodoublers; the r^2 value of the fit is shown in the Supporting Information. (c) Temporal evolution of the second harmonic intensity at the points in (a) denoted as P1, P2, and P3.

acquisition time per image. Similarly to Figure 3, the particles seem to be trapped inside the cell (which is indicated by the yellow dashed contours in Figure 4a,b. The intensity (Figure 4c) displays variations in time (with the same order of magnitude as in Figure 3), which we analyzed using an MSD algorithm and the relation between the intensity of the particle to the rotation (see the Supporting Information for a detailed description). Figure 4b shows the result of calculating the rotational diffusion for each pixel in the movie. It is clear that the various particles have different rotational diffusion coefficients, ranging from <1 deg^2/s up to 15 deg^2/s.

Summarizing the above, our work demonstrates the possibility for high resolution in vitro imaging of targeted and long term cellular processes with specificity to translational and rotational motion with acquisition times in the microsecond range. Our approach parallels certain aspects of recent advances in multiphoton optical imaging,[44] harmonic holography,[55,56] multiconfocal imaging,[57] and spatiotemporal wide field illumination:[58−61] With harmonic holography, it has been possible to image 1500 nm sized clusters of SH active particles with 100 ms acquisition time per image (with 1 mJ peak energy).[55] Single shot holography of moving particles in vitro has not been demonstrated but would be very promising. Multifocal multiphoton microscopy has been demonstrated with 1.6 ms acquisition time per image.[57] A wide field method based on spatiotemporal focusing has been used to track 500 nm fluorescent particles with 5 ms acquisition time per image in a comparable illumination area.[61] Comparatively, our approach allows us to obtain 50 μs acquisition times and hence follow accurately the rotation and translation of 100 nm nanodoublers. Given that the amount of emitted light scales with the volume of the object we believe our approach represents an important addition. The elastic nature of the light matter interaction process ensures that rotational and translational tracks can be imaged for unlimited periods of time and minimal invasion. We envisage that by employing additional appropriate functionalization with, for example, proteins and antibodies,[46] the dynamics of specific biochemical processes can be targeted with greatly increased precision.

Methods. *Cell Culture Preparation.* Human epitheloid cervix carcinoma cells were purchased from ATCC company (LGC Standards, Molsheim, France) and were grown in Dulbecco's modified Eagle's medium (DMEM, without phenol red) supplemented with 10% fetal bovine serum, 100 mg/mL streptomycin, and 100 units/mL penicillin at 37 °C with 5% CO$_2$. HeLa cells were transfected using the Neon Transfection System (Invitrogen, NY 14072, U.S.A.) following the manufacturer's instructions. Nanoparticles were introduced in the cells by electroporation, which was performed in a 6-well dish (500 000−1 000 000 cells/well) using 30 μL of nanodoublers with 0.25 mg/mL concentration dispersed in electroporation buffer. The parameters for electroporation were 1005 V. We used two pulses with a width of 35 ms. After electroporation, the cells were seeded directly onto the coverslips. Experiments were performed 24 h after transfection.

Second Harmonic Imaging System. The light source is a Yb:KGW femtosecond laser (Light Conversion Ltd.) delivering 190 fs pulses centered at 1028 nm with a 200 kHz repetition rate. The light passes through a band-pass filter (1030 nm ±10 nm, EKSPLA) and is split equally over two counter propagating beams (with a 90° angle) that are coupled into the sample chamber using a 45° prism. Each beam was polarization controlled using zero-order $\lambda/4$ and $\lambda/2$ waveplates and

focused loosely on the sample with a f = 20 cm doublet lens (Thorlabs, B coating), producing an ~100 μm beam waist diameter. The average power at the sample was set to 60−160 mW, The second harmonic photons are created in a cylindrical volume that is ~85 μm wide and 70 μm deep and imaged by a 50× objective lens (Mitutoyo Plan Apo NIR HR Infinity-Corrected Objective, 0.65 NA) in combination with a tube lens (Mitutoyo MT-L), a 800 nm short pass filer (Omega Optical), a 515 nm band-pass filter (Omega Optical, 10 nm bandwidth) and an intensified CCD camera (PiMax3 or PiMax4, Princeton Instruments). A 400 mm meniscus lens is placed behind the objective lens to remove spherical aberrations induced by the coverslip. Label-free images were recorded with the beams polarized perpendicular to the plane of the beams (SS). The readout time of the images was different because different cameras were used but can be as low as 19 μs, which is why we report on acquisition times only.

Sample Cell. The sample chamber of the cells consists of a glass window (roof) and the coverslip containing the samples (bottom) separated by a 2 mm thick Teflon ring adapted with an inlet and outlet channel. Index matching fluid (Olympus type F) is used to maximize surface contact between the prism and the roof of the chamber. The coverslip is placed in the middle of the focal volume so that the illumination depth is 70 μm.

Particle Synthesis. The synthesis of the KNbO$_3$ particles, kindly provided by Dr. Yannick Mugnier, can be found in ref 9.

Particle Characterization. TEM characterization of a single KNbO$_3$ nanoparticle was done to determine the degree of structural order and its crystallinity. Figure 1b shows TEM images taken with the microscope operating in imaging mode and in diffraction mode. Our results confirm the high crystallinity of KNbO$_3$ because clear spots are observed in the selected area electron diffraction pattern. The size distribution of the particles in solution was measured with dynamic light scattering (DLS, Malvern ZS nanosizer). The particles had a mean diameter of 107 nm with a polydispersity index (PDI) of 0.12.

Particle Tracking. Single particle tracking was performed using the TrackMate imageJ plugin as shown by Jaqaman et al.[62] Trajectories were reconstructed using a gap closing maximum distance of 4.5 μm, a maximum linking range of 2 μm, the gap closing maximum frame was set to the frame rate. Mean-square displacements (MSD) were calculated at each time value for each particle.

■ ASSOCIATED CONTENT

Ⓢ Supporting Information

The Supporting Information contains (1) details of the beam geometry, (2) information regarding the characterization of the KNbO$_3$ particles, (3) confocal images of the electroporated cells, (4) procedure for the particle tracking analysis, (5) polarization measurements of fixed KNbO3 particles, and (6) the formulas needed for the orientation particle tracking analysis. Three movies are also included: Movie 1 shows the diffusion of 100 nm KNbO$_3$ particles in water at room temperature with acquisition times of 250 μs, Movie 2 shows the rotational and translational diffusion of the same particles inside a HeLa with acquisition times of 25 ms, and Movie 3 shows the rotational diffusion of the same particles also inside a HeLa cell but with acquisition times of 50 μs. This material is available free of charge via the Internet at http://pubs.acs.org.

■ AUTHOR INFORMATION

Corresponding Authors

*aleksandra.radenovic@epfl.ch.
*sylvie.roke@epfl.ch.

Notes

The authors declare no competing financial interest.

■ REFERENCES

(1) Saxton, M. J.; Jacobson, K. *Annu. Rev. Biophys. Biomol. Struct.* **1997**, *26*, 373−99.
(2) Gu, Y.; Sun, W.; Wang, G.; Jeftinija, K.; Jeftinija, S.; Fang, N. *Nat. Commun.* **2012**, *3*, 1030−1030.
(3) Gu, Y.; Sun, W.; Wang, G.; Fang, N. *J. Am. Chem. Soc.* **2011**, 5720−5723.
(4) Mizuno, H.; Higashida, C.; Yuan, Y.; Ishizaki, T.; Narumiya, S.; Watanabe, N. *Science (New York, N.Y.)* **2011**, *331* (6013), 80−3.
(5) Dahan, M.; Levi, S.; Luccardini, C.; Rostaing, P.; Riveau, B.; Triller, A. *Science* **2003**, *302* (5644), 442−445.
(6) Gal, N.; Lechtman-Goldstein, D.; Weihs, D. *Rheol. Act.* **2013**, *52* (5), 425−443.
(7) Dempsey, W. P.; Fraser, S. E.; Pantazis, P. *Bioessays* **2012**, *34* (5), 351−360.
(8) Bonacina, L. *Molecular Pharmaceutics* **2013**, *10* (3), 783−792.
(9) Staedler, D.; Magouroux, T.; Hadji, R.; Joulaud, C.; Extermann, J.; Schwung, S.; Passemard, S.; Kasparian, C.; Clarke, G.; Gerrmann, M.; Le Dantec, R.; Mugnier, Y.; Rytz, D.; Ciepielewski, D.; Galez, C.; Gerber-Lemaire, S.; Juillerat-Jeanneret, L.; Bonacina, L.; Wolf, J. P. *ACS Nano* **2012**, *6* (3), 2542−9.
(10) McGuinness, L. P.; Yan, Y.; Stacey, A.; Simpson, D. A.; Hall, L. T.; Maclaurin, D.; Prawer, S.; Mulvaney, P.; Wrachtrup, J.; Caruso, F.; Scholten, R. E.; Hollenberg, L. C. L. *Nat. Nanotechnol.* **2011**, *6* (6), 358−63.
(11) Forkey, J. N.; Quinlan, M. E.; Shaw, M. A.; Corrie, J. E. T.; Goldman, Y. E. *Nature* **2003**, *422* (6930), 399−404.
(12) Beausang, J. F.; Sun, Y.; Quinlan, M. E.; Forkey, J. N.; Goldman, Y. E. *Cold Spring Harb. Protoc.* **2012**, *2012*, 722−725.
(13) Ohmachi, M.; Komori, Y.; Iwane, A. H.; Fujii, F.; Jin, T.; Yanagida, T. *Proc. Natl. Acad. Sci. U.S.A.* **2012**, *109* (14), 5294−8.
(14) Glass, J.; Enderle, T.; Weiss, S.; Ha, T.; Chemla, D. *Phys. Rev. Lett.* **1998**, *80*, 2093−2096.
(15) Spetzler, D.; York, J.; Daniel, D.; Fromme, R. *Biochemistry* **2006**, *45* (10), 3117−3124.
(16) Sönnichsen, C.; Alivisatos, A. P. *Nano Lett.* **2005**, *5* (2), 301−4.
(17) Chang, W.-S.; Ha, J. W.; Slaughter, L. S.; Link, S. *Proc. Natl. Acad. Sci. U.S.A.* **2010**, *107* (7), 2781−6.
(18) Wang, G.; Sun, W.; Luo, Y.; Fang, N. *J. Am. Chem. Soc.* **2010**, *132* (46), 16417−16422.
(19) Sun, W.; Wang, G.; Fang, N.; Yeung, E. S. *Anal. Chem.* **2009**, *81* (22), 9203−9208.
(20) Xiao, L.; Ha, J. W.; Wei, L.; Wang, G.; Fang, N. *Angew. Chem.* **2012**, *51*, 7734−8.
(21) Zhang, B.; Lan, T.; Huang, X.; Dong, C.; Ren, J. *Anal. Chem.* **2013**, *85* (20), 9433−8.
(22) Tcherniak, A.; Dominguez-Medina, S.; Chang, W.-S.; Swanglap, P.; Slaughter, L. S.; Landes, C. F.; Link, S. *J. Phys. Chem. C* **2011**, *115* (32), 15938−15949.
(23) Geissbuehler, M.; Bonacina, L.; Shcheslavskiy, V.; Bocchio, N. L.; Geissbuehler, S.; Leutenegger, M.; Marki, I.; Wolf, J. P.; Lasser, T. *Nano Lett.* **2012**, *12* (3), 1668−1672.

(24) Extermann, J.; Bonacina, L.; Cuna, E.; Kasparian, C.; Mugnier, Y.; Feurer, T.; Wolf, J. P. *Opt. Express* **2009**, *17* (17), 15342−15349.

(25) van den Broek, B.; Ashcroft, B.; Oosterkamp, T. H.; van Noort, J. *Nano Lett.* **2013**, *13* (3), 980−6.

(26) Xiao, L.; Qiao, Y.; He, Y.; Yeung, E. S. *J. Am. Chem. Soc.* **2011**, *133*, 10638−10645.

(27) Marchuk, K.; Fang, N. *Nano Lett.* **2013**, *13* (11), 5414−5419.

(28) Li, T.; Li, Q.; Xu, Y.; Chen, X.-J.; Dai, Q.-F.; Liu, H.; Lan, S.; Tie, S.; Wu, L.-J. *ACS Nano* **2012**, *6* (2), 1268−77.

(29) Hsieh, C. L.; Grange, R.; Pu, Y.; Psaltis, D. *Opt. Express* **2009**, *17* (4), 2880−2891.

(30) Hsieh, C.; Pu, Y.; Grange, R.; Psaltis, D. *Opt. Express* **2010**, *18* (11), 11917−11932.

(31) Yan, E. C. Y.; Eisenthal, K. B. *J. Phys. Chem. B* **2000**, *104* (29), 6686−6689.

(32) Bonacina, L.; Mugnier, Y.; Courvoisier, F.; Le Dantec, R.; Extermann, J.; Lambert, Y.; Boutou, V.; Galez, C.; Wolf, J. P. *Appl. Phys. B* **2007**, *87* (3), 399−403.

(33) Sandeau, N.; Xuan, L. L.; Chauvat, D.; Zhou, C. *Opt. Express* **2007**, *15* (24), 12−20.

(34) Pu, Y.; Grange, R.; Hsieh, C.-L.; Psaltis, D. *Phys. Rev. Lett.* **2010**, *104* (20), 207402−207402.

(35) Pantazis, P.; Maloney, J.; Wu, D.; Fraser, S. E. *Proc. Natl. Acad. Sci. U.S.A.* **2010**, *107* (33), 14535−14540.

(36) Pinaud, F.; Clarke, S.; Sittner, A.; Dahan, M. *Nat. Methods* **2010**, *7* (4), 275−85.

(37) Magouroux, T.; Extermann, J.; Hoffmann, P.; Mugnier, Y.; Le Dantec, R.; Jaconi, M. E.; Kasparian, C.; Ciepielewski, D.; Bonacina, L.; Wolf, J.-P. *Small* **2012**, *8* (17), 2752−6.

(38) Brasselet, S.; Le Floc'h, V.; Treussart, F.; Roch, J.-F.; Zyss, J.; Botzung-Appert, E.; Ibanez, A. *Phys. Rev. Lett.* **2004**, *92* (20), 207401−207401.

(39) Kachynski, A. V.; Kuzmin, A. N.; Nyk, M.; Roy, I.; Prasad, P. N. *J. Phys. Chem. C* **2008**, *112* (29), 10721−10724.

(40) Kuo, T.-R.; Wu, C.-L.; Hsu, C.-T.; Lo, W.; Chiang, S.-J.; Lin, S.-J.; Dong, C.-Y.; Chen, C.-C. *Biomat.* **2009**, *30* (16), 3002−8.

(41) Pu, Y.; Hsieh, C. L.; Grange, R.; Yang, X.; Papadopoulos, I.; Choi, J. W.; Psaltis, D. *Proc. Spie* **2011**, 8095.

(42) Ladj, R.; Kass, M. E.; Mugnier, Y.; et al. *Cryst. Growth Des.* **2012**, *12*, 5387−5395.

(43) Mayer, L.; Slablab, A.; Dantelle, G.; Jacques, V.; Lepagnol-Bestel, A. M.; Perruchas, S.; Spinicelli, P.; Thomas, A.; Chauvat, D.; Simonneau, M.; Gacoin, T.; Roch, J. F. *Nanoscale* **2013**, *5* (18), 8466−71.

(44) Hoover, E. E.; Squier, J. A. *Nat. Photonics* **2013**, *7* (2), 93−101.

(45) Culic-Viskota, J.; Dempsey, W. P.; Fraser, S. E.; Pantazis, P. *Nat. Protoc.* **2012**, *7* (9), 1618−1633.

(46) Grange, R.; Lanvin, T.; Hsieh, C. L.; Pu, Y.; Psaltis, D. *Biol. Opt. Express* **2011**, *2* (9), 2532−2539.

(47) Hsieh, C. L.; Grange, R.; Pu, Y.; Psaltis, D. *Biomaterials* **2010**, *31* (8), 2272−2277.

(48) Hsieh, C. L.; Pu, Y.; Grange, R.; Laporte, G.; Psaltis, D. *Opt. Express* **2010**, *18* (20), 20723−20731.

(49) Le Harzic, R.; Riemann, I.; König, K.; Wüllner, C.; Donitzky, C. *J. Appl. Phys.* **2007**, *102* (11), 114701−114701.

(50) Villiger, M.; Pache, C.; Lasser, T. *Opt. Lett.* **2010**, *35* (20), 3489−91.

(51) Peterson, M. D.; Hayes, P. L.; Martinez, I. S.; Cass, L. C.; Achtyl, J. L.; Weiss, E. A.; Geiger, F. M. *Opt. Mater. Express* **2011**, *1* (1), 57−57.

(52) Hunter, R. J. *Foundations of Colloid Science*; Oxford University Press: Sidney, 2002.

(53) Gomopoulos, N.; Lütgebaucks, C.; Sun, Q.; Macias-Romero, C.; Roke, S. *Opt. Express* **2013**, *21* (1), 815−815.

(54) de Beer, A. G. F.; de Aguiar, H. B.; Nijsen, J. W. F.; Roke, S. *Phys. Rev. Lett.* **2009**, *102*, 95502−95504.

(55) Pu, Y.; Centurion, M.; Psaltis, D. *Appl. Opt.* **2008**, *47* (4), A103−10.

(56) Masihzadeh, O.; Schlup, P.; Bartels, R. A. *Opt. Express* **2010**, *18* (10), 14910−14921.

(57) Bahlmann, K.; So, P. T.; Kirber, M.; Reich, R.; Kosicki, B.; McGonagle, W.; Bellve, K. *Opt. Express* **2007**, *15* (17), 10991−10991.

(58) Zhu, G.; van Howe, J.; Durst, M.; Zipfel, W.; Xu, C. *Opt. Express* **2005**, *13* (6), 2153−2153.

(59) Oron, D.; Tal, E.; Silberberg, Y. *Opt. Express* **2005**, *13* (5), 1468−1468.

(60) Choi, H.; Yew, E. Y. S.; Hallacoglu, B.; Fantini, S.; Sheppard, C. J. R.; So, P. T. C. *Bio. Opt. Express.* **2013**, *4* (7), 19645−19655.

(61) Cheng, L.-C.; Chang, C.-Y.; Lin, C.-Y.; Cho, K.-C.; Yen, W.-C.; Chang, N.-S.; Xu, C.; Dong, C. Y.; Chen, S.-J. *Opt. Express.* **2012**, *20* (8), 8939−48.

(62) Jaqaman, K.; Loerke, D.; Mettlen, M.; Kuwata, H.; Grinstein, S.; Schmid, S. L.; Danuser, G. *Nat. Methods* **2008**, *5* (8), 695−702.